Hindawi
Geofluids
Volume 2020, Article ID 6656460, 11 pages
https://doi.org/10.1155/2020/6656460

Research Article

Quantitative Investigation on the Contributing Factors to the Contact Angle of the CO_2/H_2O/Muscovite Systems Using the Frumkin-Derjaguin Equation

Masashige Shiga,[1,2] **Masaatsu Aichi**,[2] **and Masao Sorai**[1]

[1]*Institute for Geo-Resources and Environment, National Institute of Advanced Industrial Science and Technology, Tsukuba, Japan*
[2]*Department of Environment Systems, Graduate School of Frontier Sciences, The University of Tokyo, Kashiwa, Japan*

Correspondence should be addressed to Masashige Shiga; shiga.masashige@envsys.k.u-tokyo.ac.jp

Received 7 October 2020; Accepted 7 November 2020; Published 24 November 2020

Academic Editor: Mohamed A. El-Beltagy

It is significant to understand the values and trends of the contact angle of CO_2/brine/mineral systems to evaluate and model the sealing performance of CO_2 Geo-Sequestration (CGS). It has been reported that the contact angles of the CO_2/brine/muscovite systems increase as pressure increases from ambient conditions to reservoir conditions. This trend suggests a decrease in seal integrity. In this paper, we studied its mechanisms and the contributing factors by calculating the Frumkin-Derjaguin equation, which is based on the thermodynamics of the interfacial system. Results show that a decrease of pH is a critical factor for the wettability alteration at a lower pressure range (0.1 MPa to 3.0 MPa). In contrast, the increase of CO_2 density and the decrease in the interfacial tension of CO_2/brine are significant for the wettability change at a higher pressure range (3.0 MPa to 10.0 MPa). Also, sensitivity analysis shows that the contact angle is sensitive to the interfacial tension of CO_2/brine and the coefficients of hydration forces.

1. Introduction

CO_2 Geo-Sequestration (CGS) and CO_2-EOR (enhanced oil recovery) are crucial strategies to pursue sustainable development. Reservoir rocks and caprocks typically consist of fine mineral particles from micrometer to nanometer sizes [1]. In such porous media, the interfacial phenomena have crucial roles in the multiphase fluid flow because of the high specific surface area. Wettability is a critical factor because it directly influences sealing performance in CGS and the oil-recovery rate in CO_2-EOR [2].

Contact angle θ is an indicator of wettability. Many measurements of CO_2/brine/mineral systems have been carried out using muscovite, quartz, and calcite, which are essential minerals for caprock or reservoir rock. It has been reported that the contact angle of the CO_2/brine/muscovite systems increases as pressure (of CO_2 or an experimental system) increases [3–6]. Although the absolute values are different among these studies, the overall trend is consistent with each other. Increases in the contact angle may decrease the sealing performance and the storage potential. As a key mechanism of this trend, changes in pH and CO_2 density are suggested by previous studies [3–5]. However, these effects have not been quantitatively studied.

The contact angle is determined by the balance of one interfacial tension and two interfacial energy terms: CO_2/brine, brine/mineral, and CO_2/mineral. Then, it is worth paying attention to the properties of each interface in order to understand the mechanism of the change in contact angle. The thermodynamic model on these interfaces is helpful to quantitatively evaluate which property contributes to the change in the contact angle. Establishing a quantitative model helps interpret and estimate differences in sealing performance at different physical properties and conditions.

Several studies have calculated the contact angle for oil/-brine/mineral systems at the thermodynamic equilibrium [7–9] based on the Frumkin-Derjaguin equation [10, 11]. In the thermodynamic equilibrium state, brine in the wetting

phase forms a thin adsorption film. The disjoining pressure acting on the water film consists of van der Waals forces, electrostatic forces, and hydration forces (structural forces).

In this study, by using the Frumkin-Derjaguin equation, we studied the mechanisms of the change of the contact angles of the CO_2/brine/muscovite systems by increasing pressure and investigated the contributing factors quantitatively.

2. Materials and Methods

2.1. Contact Angle Calculation by the Frumkin-Derjaguin Equation. Contact angle θ is determined by the balance of three interfacial tensions (IFT) or surface energy in the case of fluid/solid interfaces. It is formulated with Young's equation (equation (1)), showing the mechanical equilibrium of IFT and surface energy:

$$\mathrm{Cos}\theta = \frac{\gamma_{\mathrm{CM}} - \gamma_{\mathrm{BM}}}{\gamma_{\mathrm{BC}}}, \tag{1}$$

where γ_{BC}, γ_{CM}, and γ_{BM} are IFT of brine/CO_2, interfacial energy of CO_2/mineral, and interfacial energy of brine/mineral, respectively. θ is zero when $\gamma_{\mathrm{CM}} - (\gamma_{\mathrm{BM}} + \gamma_{\mathrm{BC}}) \geq 0$, while the system has a finite value of θ when $\gamma_{\mathrm{CM}} - (\gamma_{\mathrm{BM}} + \gamma_{\mathrm{BC}}) < 0$. The latter means the partial wetting state. Young's equation is valid in the mechanical equilibrium condition. In order to formulate a contact angle in the thermodynamic equilibrium condition, however, it is necessary to consider the effect of water adsorption. γ_{CM} decreases because H_2O adsorbs to lower the free energy of the system. By adsorption of H_2O, the distance between CO_2 and the mineral increases. The force acting between two interfaces (CO_2/brine and brine/-mineral) of the film balances the capillary pressure. This force acting on the film per unit area is a disjoining pressure and is related to the stability of the film [7]. Finally, a contact angle is calculated by equation (2), called the Frumkin-Derjaguin equation [7, 10, 11]:

$$\mathrm{Cos}\theta = 1 + \frac{1}{\gamma_{\mathrm{BC}}}\int_0^{\Pi(h_{\mathrm{eq}})} h'\,d\Pi' = 1 - \frac{1}{\gamma_{\mathrm{BC}}}\left[\int_\infty^{h_{\mathrm{eq}}} \Pi(h)dh - h_{\mathrm{eq}}\Pi\left(h_{\mathrm{eq}}\right)\right], \tag{2}$$

where h is the film thickness, h_{eq} is the film thickness in thermodynamic equilibrium, and Π is the disjoining pressure.

2.2. Formulation of Disjoining Pressure. Disjoining pressure is modeled considering the DLVO theory and structural forces [7]. The DLVO theory describes the balance between van der Waals forces and electrostatic forces. Hydration forces are non-DLVO forces and represent short-range forces between hydrophilic surfaces or hydrophobic surfaces, which are essential in the stability of colloid particles or a soap film [12]. Disjoining pressure Π is formulated by these three terms shown in equation (3). h means the thickness of the water film between the CO_2 phase and the mineral phase.

$$\Pi(h) = \Pi_{\mathrm{vdW}}(h) + \Pi_{\mathrm{ele}}(h) + \Pi_{\mathrm{hyd}}(h). \tag{3}$$

The integration of $\Pi(h)$ is defined as follows:

$$W(h) = -\int_\infty^h \Pi(h)dh, \qquad W(h) = W_{\mathrm{vdW}}(h) + W_{\mathrm{ele}}(h) + W_{\mathrm{hyd}}(h). \tag{4}$$

2.2.1. Van der Waals Forces.

$$\Pi_{\mathrm{vdW}}(h) = -\left(\frac{A}{6\pi h^3}\right). \tag{5}$$

The coefficient A of the van der Waals interaction is the Hamaker constant. When $A > 0$, this interaction acts as attractive forces. As shown in equation (6), the Hamaker constant of CO_2 and H_2O can be calculated from the Lifshitz theory using experimental data of the refractive index and the relative permittivity. A_{ii} means the constant for material i is interacting across a vacuum.

$$A_{ii} = \frac{3}{4}k_{\mathrm{B}}T\left(\frac{\varepsilon_i - 1}{\varepsilon_i + 1}\right)^2 + \frac{3h'\nu_{\mathrm{e}}}{16\sqrt{2}}\frac{\left(n_i^2 - 1\right)^2}{\left(n_i^2 + 1\right)^{3/2}}, \tag{6}$$

where k_{B} is the Boltzmann constant, T is the temperature, ε_i is the relative permittivity of material i, h' is the Planck constant, ν_{e} is the main electronic absorption frequency, n_i is the refractive index of material i, and the material numbers of minerals, CO_2, and H_2O are 1, 2, and 3, respectively. The Hamaker constant of muscovite is determined from experimental data, as summarized in Table S1. Several existing studies [13–18] reported the value around 1.0×10^{-19} J. This value is used in this study for A_{11}. Finally, the Hamaker constant of the water film sandwiched between the CO_2 phase and the mineral phase (A_{132}) is calculated from A_{11}, A_{22}, and A_{33} based on the mixing rule:

$$A_{132} = A_{12} + A_{33} - A_{13} - A_{23} = \left(\sqrt{A_{11}} - \sqrt{A_{33}}\right)\left(\sqrt{A_{22}} - \sqrt{A_{33}}\right) = \left(\sqrt{A_{11}} - \sqrt{A_{33}}\right)\left(\sqrt{A_{22}} - \sqrt{A_{33}}\right). \tag{7}$$

Values of ε_i and n_i at conditions for the calculation of equation (6) followed existing studies [19–23]. In this calculation, A_{11} is assumed to be constant with increasing pressure. The changes in the optical properties ε_i and n_i of minerals are usually negligible within the pressure and temperature ranges in this study. For example, the optical properties of sapphire change less than 0.5% when the pressure increases from 0.0 Pa to 10.0 GPa [24].

2.2.2. Electrostatic Forces. The contribution from the electrostatic forces is calculated from equation (8) [25–27]. The constant potential (CP) model or the constant charge (CC) model is used to formulate the interaction of two dissimilar surfaces in electrolyte solutions. These models assume that the surface electrical potential or surface charge is constant when two surfaces approach. Each of them is calculated from the minus sign and the plus sign of equation (8), respectively.

In reality, both potential and charge are likely to change as the interfaces approach each other. Between these two models, different contact angles can be obtained from one single pair of surface potentials ϕ_{BC} and ϕ_{BM}. Therefore, in this work, in order to evaluate the effect of the model, calculations are conducted by both CP and CC models:

$$\Pi_{ele}(h) = \frac{1}{2}\varepsilon_0\varepsilon\kappa\Phi_{BM}^2\left[\pm\left(1+F_\Phi^2\right)\kappa(\operatorname{csch} h_D)^2 + 2\kappa F_\Phi \operatorname{csch} h_D \coth h_D\right], \tag{8}$$

where

$$\kappa = e^2\sum\frac{C_i z_i{}^2}{\varepsilon_0\varepsilon kT},$$
$$h_D = \kappa h, \tag{9}$$
$$F_\phi = \frac{\phi_{BC}}{\phi_{BM}}.$$

e is the elementary charge, C_i is the concentration of i (molecules/m^3), and z_i is the valence of ion i.

ε_0 is the permittivity of vacuum, ε is relative permittivity, and κ is reciprocal Debye length. ϕ_{BC} and ϕ_{BM} are surface electrical potentials of brine/CO_2 and brine/muscovite, respectively. F_ϕ is the ratio of these two potentials. h_D is the dimensionless distance. In this work, the data of the zeta potential of brine/muscovite [28–30] and brine/CO_2 [31] are used as the parameters in Π_{ele}.

2.2.3. Hydration Forces. In 2019, Van Lin et al. measured the hydration forces acting on mica surfaces and determined parameters in empirical formulations at different ions, salinity, and pH. The empirical model consists of two terms: monotonically exponential decaying curve and the decaying oscillation curve [32]. The disjoining pressure is determined by their magnitudes and the decay lengths [33], so Π_{hyd} is obtained as follows:

$$\Pi_{hyd}(h) = K_m/\lambda_m \exp(-h/\lambda_m) + K_{osc}/\lambda_{osc}\cos(2\pi\sigma h - \varphi)\exp(-h/\lambda_{osc}), \tag{10}$$

where K_m and K_{osc} are the coefficients of the monotonical and oscillated decaying of the hydration forces. λ_m and λ_{osc} are the decay lengths of the monotonical and oscillated decaying of the hydration forces. σ and φ are the structural hydration frequency and the phase shift.

2.3. The Augmented Young Laplace Equation. The equilibrium thickness h_{eq} of the film is determined from the augmented Young Laplace equation. Provided that the CO_2/brine/muscovite system with the brine film between CO_2 and the muscovite are as shown in Figure 1, the augmented Young Laplace equation holds at the equilibrium state and is described as follows:

$$P_c = \frac{2\gamma_{BC}}{R} + \Pi(h), \tag{11}$$

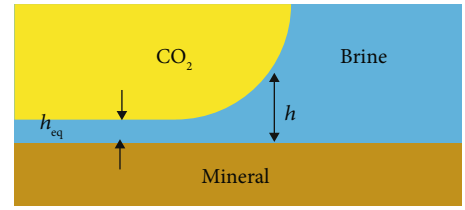

Figure 1: Conceptual model of the interfacial region of the CO_2/brine/mineral system; h is the film thickness, and h_{eq} is the equilibrium thickness of the water adsorption film. This thickness is determined from the relation between the capillary pressure and the disjoining pressure.

where R is the curvature radius of the interface of brine/CO_2, and P_c is the capillary pressure. 60 kPa is assumed as the base case of P_c. Assuming a typical droplet radius for the contact angle measurement, the Laplace pressure acting on the droplet was set as the value of P_c. The effect of P_c on θ is small enough to be neglected in this study though it must be included if the size of the droplet is of nanometer order because the Laplace pressure can be as high as MPa order. In the flat film region, $1/R = 0$ and equation (11) becomes equation (12):

$$P_c = \Pi(h_{eq}). \tag{12}$$

The flat film has a thickness h_{eq} in the equilibrium state, and the equilibrium contact angle θ can be calculated by equation (2). There can be multiple thicknesses which satisfy equation (12). In addition, the thin film at the thermodynamic equilibrium condition must be locally stable. Such a local stable state holds where $\partial\Pi(h)/\partial h < 0$, that is, $\Pi(h)$ has a negative slope at the thickness [7]. Then, the trend of θ at all stable films is studied.

2.4. The Potential Energy of the Film. The system has a finite value of θ when the integration part $\int_0^{\Pi(h_{eq})} h'\,d\Pi'$ is negative. This integration is the potential energy required to form the film from infinite separation to the equilibrium thickness h_{eq} [7]. Based on equation (2), as shown in Figure S1(a), when the area of the blue part ($\Pi(h) < 0$) is larger than that of the red region ($\Pi(h_{eq}) \geq \Pi(h) \geq 0$), $\cos\theta$ is smaller than 1 and the system is in a partial wetting state. On the other hand, when the red region is larger than the blue region as shown in Figure S1(b), the system is in a complete wetting state. So, the negative disjoining pressure (attractive force) leads to an increase in the contact angle, and the positive disjoining pressure (repulsive force) leads to a decrease in the contact angle. By considering these models and mechanisms on the wetting state, the effects of the physical properties of CO_2, brine, and minerals can be evaluated and discussed.

2.5. Calculation Condition. In this work, we compare three pressure values, namely, 0.1, 3.0, and 10.0 MPa, at constant temperature (313 K) to study the effect of increasing pressure. 0.1 MPa represents the ambient pressure condition, 3.0 MPa

Table 1: Parameters for calculation of the contact angle at 0.1 MPa, 3.0 MPa, and 10.0 MPa.

Parameter	0.1 MPa	3.0 MPa	10.0 MPa
Hamaker constant A_{11} (J)	1.0×10^{-19}	1.0×10^{-19}	1.0×10^{-19}
Hamaker constant A_{22} (J)	5.52×10^{-26}	6.63×10^{-23}	7.33×10^{-21}
Hamaker constant A_{33} (J)	3.38×10^{-20}	3.38×10^{-20}	3.40×10^{-20}
Hamaker constant A_{132} (J)	-2.43×10^{-20}	-2.33×10^{-20}	-1.30×10^{-20}
Salinity (mol/kg)	0.01	0.01	0.01
pH	5.0	3.37	3.24
γ_{BC} (mN/m)	68.0	50.0	32.0
ϕ_{BC} (mV)	-16.4	-15.1	-15.0
ϕ_{BM} (mV)	-12.7	2.4	3.5
Capillary pressure (kPa)	60.0	60.0	60.0

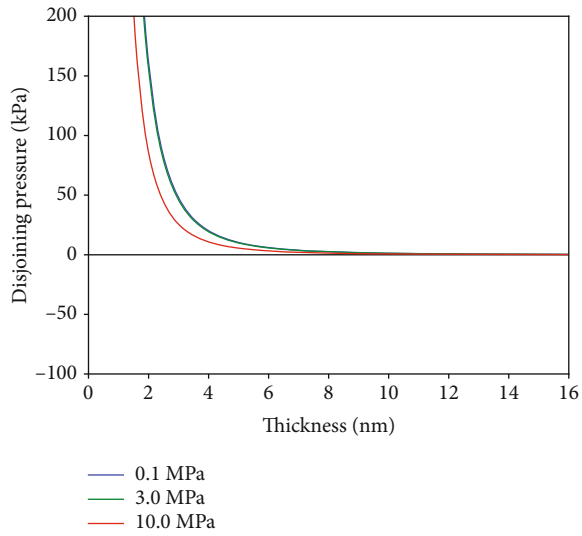

Figure 2: Dependence of $\Pi_{vdW}(h)$ on the Hamaker constant A_{132}. For the water film sandwiched between CO_2 and muscovite, A_{132} is negative and repulsive forces act on the film. The decrease in the repulsive forces lead to the decrease in the integration part $\int_0^{\pi(h_{eq})} h' d\Pi'$ (the red colored area in Figures S1 and S2). This means that increasing pressure leads the system to being less water wet (increase in the contact angle). A_{132} for each pressure is from Table 1.

a high pressure but lower than the critical point (7.38 MPa), and 10.0 MPa a supercritical state of CO_2. Also, 10.0 MPa and 313 K are typical pressure and temperature conditions for reservoir formations at 1 km depth. Physical properties at each pressure are listed in Table 1.

3. Results and Discussion

By focusing on each component of disjoining pressure (Π_{vdW}, Π_{ele}, Π_{hyd}) in equation (3) using parameters of CO_2, brine, and muscovite, the contact angles were calculated, and the mechanisms of its change are discussed below.

3.1. Van der Waals Forces. In Figure 2, the pressure dependency of the disjoining pressure of the van der Waals forces at several values of the Hamaker constant was plotted. The absolute value of the forces becomes larger as the distance between the two surfaces becomes smaller. In the case of $A_{132} < 0$, the van der Waals forces are positive and act as repulsive forces. Based on equations (6) and (7), A_{132} at 0.1 MPa, 3.0 MPa, and 10.0 MPa are -2.43×10^{-20} J, -2.33×10^{-20} J, and -1.33×10^{-20} J, respectively. This indicates that van der Waals forces become less repulsive, and the system becomes less water wet, with increasing pressure. Therefore, the change in Π_{vdW} by increasing pressure is one of the causes of the increase in the contact angle of the CO_2/brine/-muscovite system.

This trend of A_{132} with increasing pressure is related to the fact that the density of CO_2 increases more rapidly than that of H_2O. Optical properties of molecular structures ε_i and n_i, on which the Hamaker constant largely depends, increase linearly with the increasing densities of H_2O and CO_2 [19–23]. As seen in Figure S2, CO_2 density increases considerably more than H_2O density with increasing pressure, and this is seen in the trend of A_{22} and A_{33} (data of density is from Lemmon et al. [34]). A_{11}, A_{22}, and A_{33} are constant or increase with an increase in pressure. A_{132} is negative and decreases in magnitude $|A_{132}|$ with an increase in pressure. Among the three materials, only CO_2 drastically changes its density, and this is reflected in the trend of each of Hamaker constant.

3.2. Electrostatic Forces. Equation (8) indicates that Π_{ele} can be affected by several parameters: relative permittivity and salinity of brine and surface electrical potentials. A change of the relative permittivity in the pressure range of 0.1 MPa ~ 10.0 MPa is small enough to be neglected, judging from its dependence on pressure [35], unlike CO_2, which changes density drastically and changes the relative permittivity. Surface electrical potentials and charges are, on the other hand, primarily affected by pH change, and even the sign can change.

In Figures S4 and S5, Π_{ele} at several values of surface electrical potentials calculated by the CP and CC models are shown, respectively. Those at different pressures (0.1,

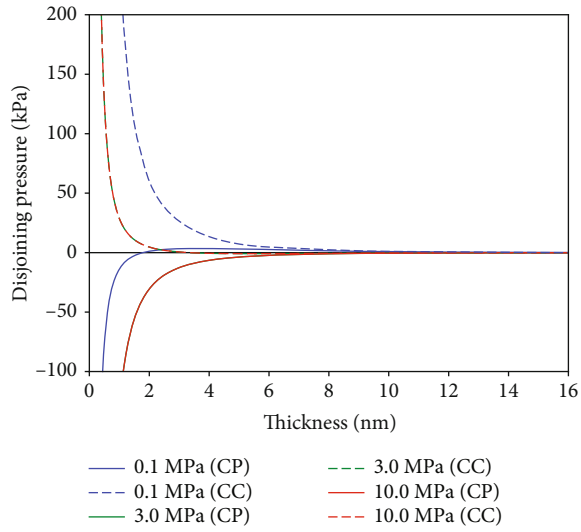

Figure 3: Π_{ele} at each system pressure calculated from both the CP model (solid line) and the CC model (dashed line).

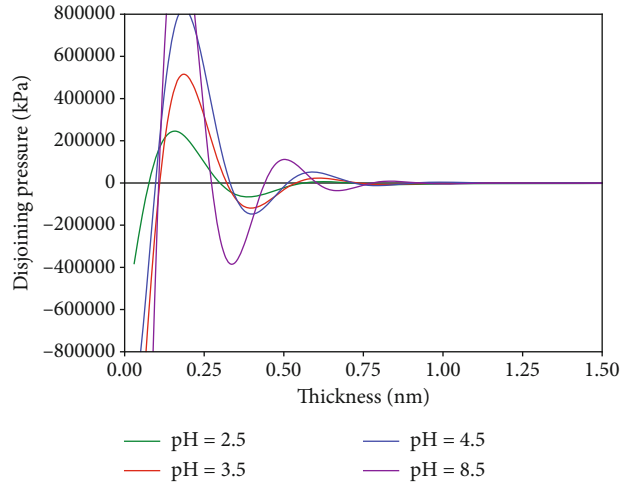

Figure 4: Hydration forces $\Pi_{hyd}(h)$ at different pHs (2.5, 3.5, 4.5, and 8.5) based on the hydration force curves [32].

3.0, and 10.0 MPa) are shown in Figure 3. The shapes of the curves are dependent on the model choice, as summarized in Table S2. In order to evaluate the contact angle by this framework, its dependence on the model choice must be studied.

With increasing pressure in the CO_2/H_2O two-phase system, the pH decreases from 6 ~ 7 to 2 ~ 3. pH is 3.37 and 3.24 at 3.0 MPa and 10.0 MPa, respectively [36]. By lowering pH from 5.0 to 3.5, ϕ_{BC} increases from -18.0 mV to -15.0 mV [37]. In this pH range, charge reversal happens for the H_2O/muscovite surface [28–30]. ϕ_{BM} is -10.0 mV at pH 5.0, while it increases to around +5.0 mV at pH 3.5. This indicates that ϕ_{BC} and ϕ_{BM} have the same signs at low pressure (0.1 MPa), while they have opposite signs at high pressure (3.0 MPa and 10.0 MPa). They do not change much between 3.0 MPa and 10.0 MPa, so curves of these two pressure conditions are almost the same in Figure 3. In Figure 3, although Π_{ele} in the CP model acts as attractive forces while that in the CC model acts as repulsive forces, the trend by increasing pressure is the same; the integration of equation (2) decreases, and it leads to an increase in the contact angle. Therefore, lowering pH from 5.0 to 3.5 leads to being less water wet because the negative area of Π_{ele} increases, as seen in Figure 3. The change of Π_{ele} is one of the causes for increasing θ when the pressure increases from ambient pressure to the high-pressure range on the order of MPa.

3.3. Hydration Forces. Since it is not easy to measure hydration forces directly under high pressure, there is no data at high pressures of interest. Hydrating forces are short-range interactions that act at a few nanometers on the mineral surface and are strongly dependent on the adsorption structure. Changes in density and pH can be considered as influential factors as a result of pressure changes. However, since the density change of water is less than 0.4% (992.27 kg/m^3 to 996.57 kg/m^3) from 0.1 MPa to 10.0 MPa, the sensitive parameter is pH.

In 2019, Van Lin et al. developed an empirical formulation based on their measurements of hydration forces of mica surfaces. Π_{hyd} at several pHs (2.5, 3.5, 4.5, and 8.5) are shown in Figure 4. In order to see the effect of pressure, $\Pi_{hyd}(h)$ at pH = 4.5 is regarded as the case of 0.1 MPa, and $\Pi_{hyd}(h)$ at pH = 3.5 is for the case of 3.0 MPa and 10.0 MPa. By lowering pH, amplitudes of the oscillation $|K_{osc}|$ decrease, and attractive interactions develop. In Figure S4, the integration $\int_h^\infty \Pi_{hyd}(h)dh$ is plotted. The curve for pH = 3.5 (red curve in Figure S4) is smaller than that for pH = 4.5 (blue curve in Figure S4). This results in less wetting of the system.

Note that the pH drops from 3.37 to 3.24 when the pressure changes from 3.0 MPa to 10.0 MPa. Comparing pH 3.5 and pH 2.5, the negative region of Π_{hyd} was greatly increased. Therefore, a slight decrease in pH in the higher pressure region (order of MPa) is considered to be significant on the increase in contact angle. The attractive force significantly increased.

3.4. Total Disjoining Pressure. Figure 5 shows the total disjoining pressure Π_{tot} and the integration $\int_h^\infty \Pi_{tot}(h)dh$ at different pressures of the system: 0.1 MPa, 3.0 MPa, and 10.0 MPa. Physical properties at each case are listed in Table 1. The orange-colored dashed horizontal line in Figure 5 represents the value of P_c (60 kPa). Thicknesses at which the integration has a local minimum or maximum correspond to thicknesses where the disjoining pressure is equal to the capillary pressure (equation (12)). Among them, the blue circles in Figure 5 are stable films, which satisfy $\partial\Pi(h)/\partial h < 0$. The system can have contact angles at points h_{eq1} (thinner) and h_{eq2} (thicker). Each case calculated by both the CP (solid curve) and CC (dashed curve) models for Π_{ele} is drawn. W_{tot} on the model choice does not much affect the results of the equilibrium thickness and the stability of the film. The thickness of the thinner film is from 0.326 nm to 0.339 nm, and that of the thicker film is from 0.728 nm to 0.749 nm (see Table S3). These correspond to those of the structured water adsorption layer on muscovite, by X-ray

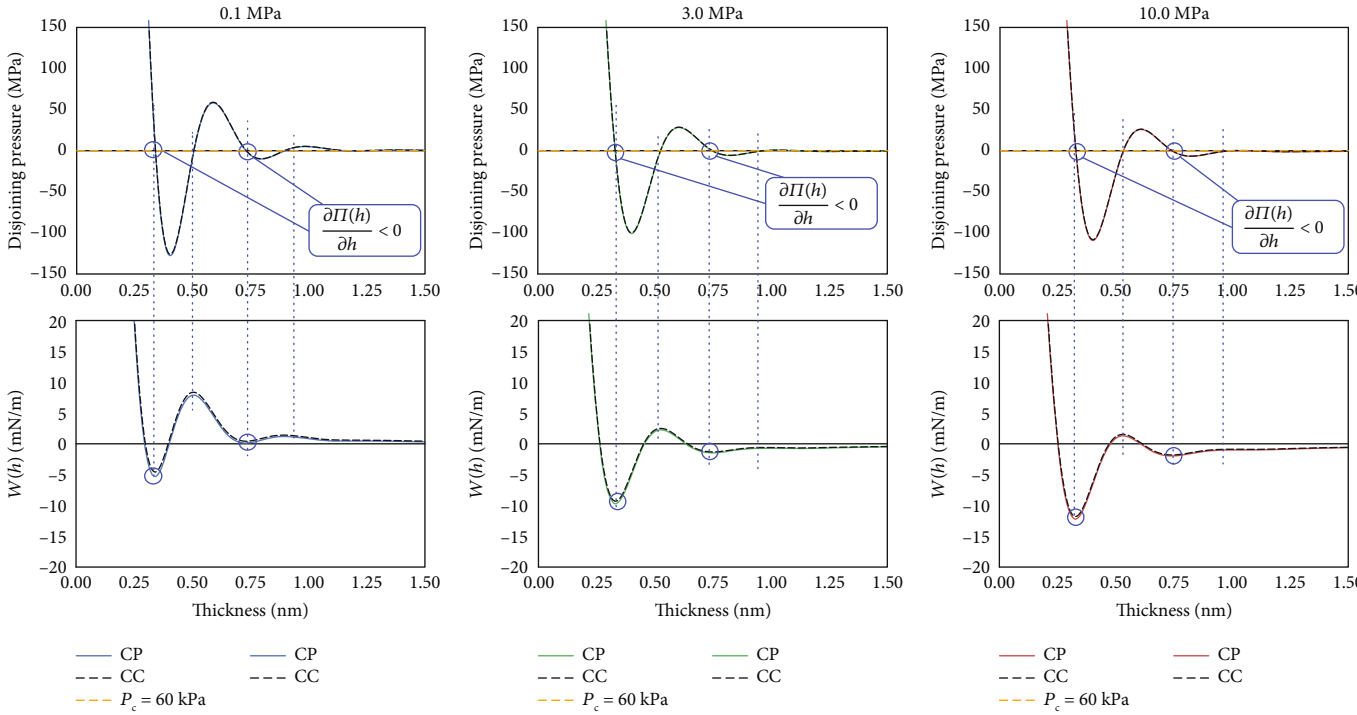

Figure 5: Total disjoining pressure and its integration at each pressure are shown. Curves calculated by both the CP and CC models are shown. Dashed and orange-colored horizontal lines in the upper figures show $P_c = 60.0$ kPa. The local minimum of integration decreases with increasing pressure. This decreases cos θ and leads to being less water wet.

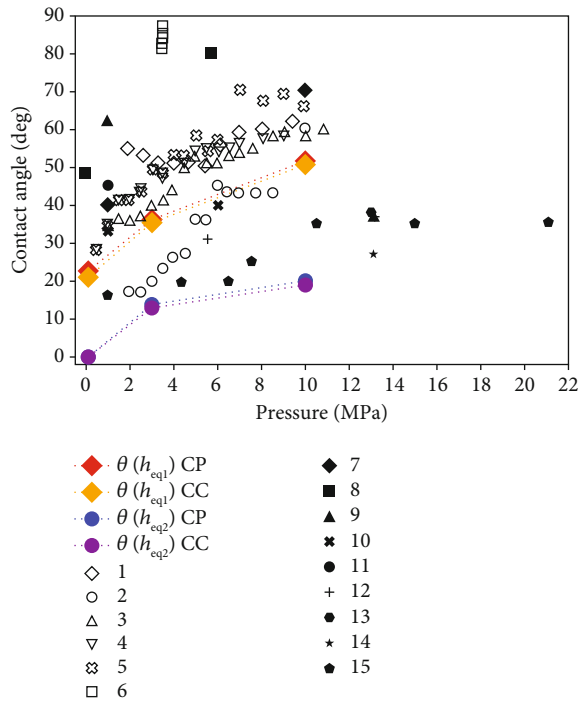

Figure 6: Results of calculation (colored plots) and experimental data of the contact angle of the CO_2/brine/muscovite system; plots of experimental data are modified from Iglauer et al. The numbers (1 to 15) of references in the legend are shown in Table 2.

CTR measurement [37–39] and molecular dynamics simulation [40, 41]. Differences of $W_{tot}(h_{eq1})$ and $W_{tot}(h_{eq2})$ between the CP and CC models are less than 0.74 mN/m and 0.30 mN/m, respectively. These are small enough to affect the results of the contact angle because values of γ_{BC} in equation (2) are from 68 mN/m to 32 mN/m in the pressure conditions.

Each term of Figure 5 at each pressure is shown in Figure S5. At the pressure of 0.1 MPa, the thicker film has zero contact angle, i.e., it is completely water wet. With increasing pressure, the local minimum of the integration decreases. This leads to an increase in θ with increasing pressure both at thinner and thicker films. All values of h_{eq} and $W(h_{eq})$ are summarized in Table S3 and Table S4.

From 0.1 MPa to 3.0 MPa, the increase in the attractive forces of Π_{ele} and Π_{hyd} has led to the overall decrease in the integration part $\int_h^\infty \Pi_{hyd}(h)dh$ and the local minimum. 93.0% (CP model) and 87.3% (CC model) of the decreases in $W_{tot}(h_{eq1})$ are caused by the decrease in W_{hyd}, and 84.2% and 77.4% of the decreases in $W_{tot}(h_{eq2})$ are caused by the decrease in W_{hyd}.

From 3.0 MPa to 10.0 MPa, 93.3 ~ 93.8% of the decreases in $W_{tot}(h_{eq1})$ and $W_{tot}(h_{eq2})$ are caused by the change in W_{vdW} because the curves of Π_{ele} slightly change, and Π_{hyd} is the same at these two pressures because pH at these pressures is almost the same. Although detailed quantification of the reduction of Π_{hyd} from pH 3.37 to 3.24 was not done in this work, the data from the hydration curves of Van Lin

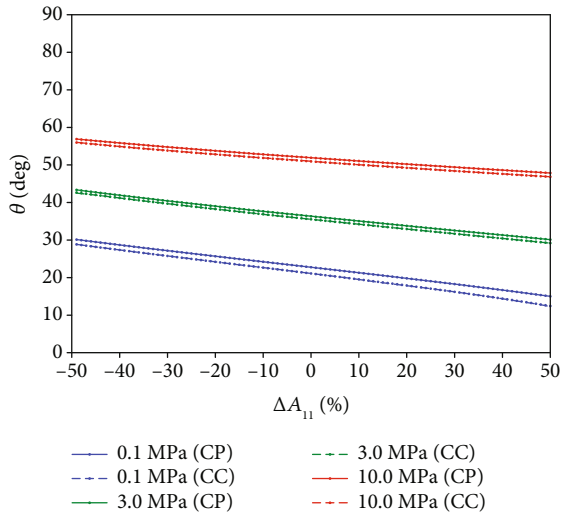

Figure 7: The contact angle with changes of the Hamaker constant A_{11}.

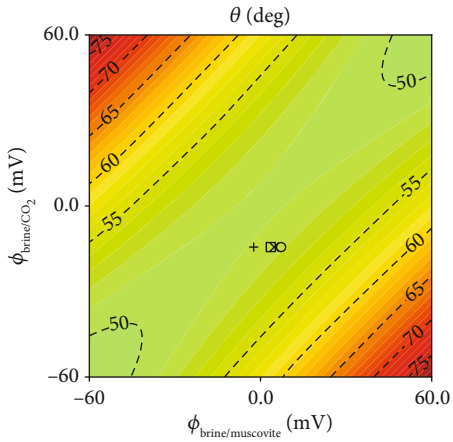

Figure 8: The contact angle with changes in the surface electrical potentials. "□" shows the value calculated from the base case at Table 1. "×", "○", and "+" indicate values calculated from each different reported value [28–30].

et al. in 2019 show that attraction from pH 3.5 to pH 2.5 increases significantly. Therefore, it is considered that the change in Π_{hyd} from pH 3.37 (3.0 MPa) to pH 3.24 (10.0 MPa) has a greater effect on the increase in contact angle than estimated here.

3.5. Effect of the Interfacial Tension of CO_2/Brine. The interfacial tension of CO_2/brine surface γ_{BC} is included in equation (2). γ_{BC} decreases with increasing pressure. As can be seen in equation (2), a decrease of γ_{BC} decreases $(1/\gamma_{BC})\int_0^{\pi(h_{eq})} h' d\Pi'$ (<0), which leads to a decrease in cos θ, that is, increases in θ. For example, when the pressure increases from ambient pressure to 3.0 MPa, γ_{BC} decreases from 68 mN/m to 50 mN/m (26.4% decrease). From 3.0 MPa to 10.0 MPa, it decreases from 50 mN/m to 32 mN/m (36.0% decrease) (the temperature is 312.9 K, and pure H_2O is used) [42]. This decrease drastically affects θ.

3.6. Contact Angle. By calculating each component in equation (3), θ is obtained from equation (2), as plotted in Figure 6. θ at both thinner and thicker films increased with increasing pressure. This corresponds to the increasing trend seen in existing measurements. Key factors of this trend were (a) a decrease of repulsive van der Waals forces, (b) charge reversal for the two surfaces, (c) increase of attraction of the hydration forces, and (d) decrease in γ_{BC}. (b) and (c) are especially important for the change in the lower pressure range from 0.1 MPa to 3.0 MPa. (a) and (d) were influential in the whole range of the targeted pressure, but it drastically affected results within the higher pressure range from 3.0 MPa to 10.0 MPa. Since Π_{tot} and W_{tot} calculated by the CP and CC models for Π_{ele} are not much different, the model choice does not much affect the values and the trend of the contact angle. Results obtained by the CC model are 1.16° to 1.45° smaller than those by the CP model because Π_{ele} remains positive (repulsive) as the film becomes thinner, as shown in Figure 3.

Sensitivity analysis was carried out about parameters of disjoining pressure.

In Figure 7, the effect of the Hamaker constant of muscovite A_{11} on the contact angle at the thinner film is plotted. Although the Hamaker constants of water and CO_2 are accurately determined from their densities, that of muscovite has differences between reported values. The range of reported data of A_{11} is from 6.96×10^{-20} J [44] (-30.4% of ΔA_{11} in Figure 7) to 1.35×10^{-19} J [14] (+35.0% of ΔA_{11} in Figure 7). Changes in the contact angle values due to these differences are less than 10.5°, 8.7°, and 6.2° at each of the three pressures. Variations of these data affect the calculation results, especially in lower pressure ranges because $(\sqrt{A_{22}} - \sqrt{A_{33}})$ in equation (7) is larger and A_{11} changes A_{132} more directly.

In Figure 8, by using the CP model, a 2D map of the contact angle at the thinner film was plotted as a function of ϕ_{BM} and the vertical axis as ϕ_{BC}. In this map, other parameters except for ϕ_{BC} and ϕ_{BM} are constant based on physical properties at 10.0 MPa. Maps at other pressure conditions are shown in Figures S11 and S12. As mentioned in the introduction of Π_{ele}, when the two surfaces charge oppositely, attractive forces act to decrease the potential energy of the film, which is the integration part of equation (2), and θ becomes higher. On the other hand, when these have the same sign of the surface charge, θ becomes smaller. Charge reversal of two surfaces of the brine film, from the same signs to the opposite signs, is a key mechanism of the contact angle alteration of the oil/brine/mineral systems [45]. In this study, the averaged value of three zeta potential values of brine/muscovite using data from Alonso et al. [28], Au et al. [29], and Zhou et al. [30] were used for ϕ_{BM}, and data from Kim and Kwak [31] was used for ϕ_{BC}. In these maps, contact angles calculated from each ϕ_{BM} are plotted. Differences in the values are less than 2.0°. Also, it can be estimated that the difference of ϕ_{BC}, which is less than 10 mV, causes the change in the contact angle to less than 2.0° at each ϕ_{BM}.

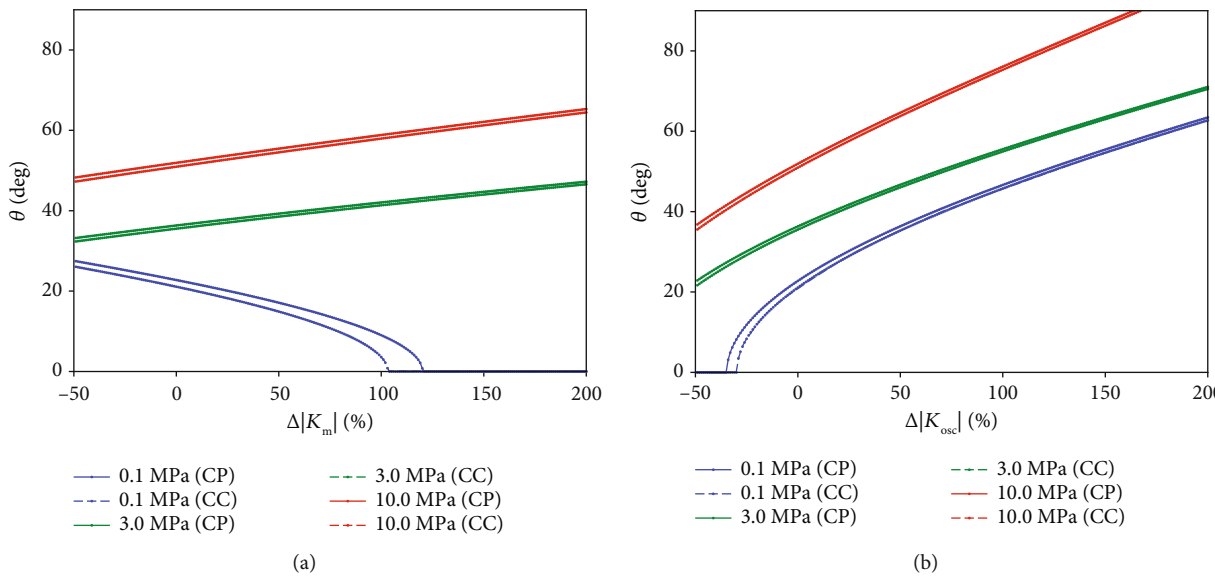

Figure 9: (a) Sensitivity analysis of the magnitude of the monotonic term of the hydration forces. (b) Sensitivity analysis of the magnitude of the oscillation term of the hydration forces.

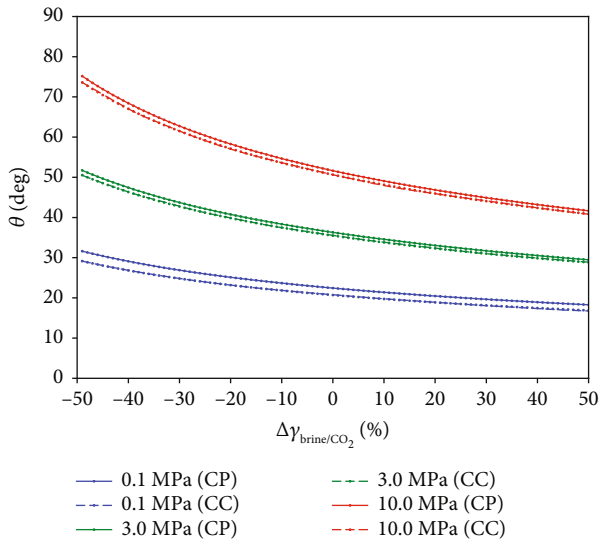

Figure 10: Sensitivity analysis of IFT of CO_2/brine.

In Figure 9, dependencies of the contact angles on the coefficients of hydration forces were plotted. Variations of the magnitudes at pH 3.5 and 4.5 are probably within the range of values at pH from 2.5 to 8.5. Sensitivity analysis was carried out in these ranges using parameters by Van Lin et al. [32]. Both magnitudes can change from half to twice of those at pH 3.5 or 4.5, so the horizontal axis is from -50% to 200%. Results show that θ can be drastically changed by changing these magnitudes.

In addition to physical properties related to the disjoining pressure, the sensitivity of IFT of CO_2/brine on the contact angle at the thinner film is studied here. Although many measurements have been performed for CO_2/brine IFT, there are variations depending on the reported results. On the other hand, Georgiadis et al. [42] pointed out problems with conventional measurement methods (about 40% of underestimation may occur [42]) and they measured the IFT value by a more accurate method. This led us to use their data in this study. However, as can be seen from equation (2), IFT directly affects $\cos\theta$, and it can be a sensitive parameter. In Figure 10, the effects of changes in IFT are shown quantitatively. Sensitivity is higher in higher pressure. When the IFT error is less than 10% (6.8 mN/m, 5.0 mN/m, and 3.2 mN/m at 0.1 MPa, 3.0 MPa, and 10.0 MPa), the effect on the contact angle is less than 1.2°, 2.0°, and 3.1°, respectively. The contact angle may increase by about 9°, 15°, and 23° at each of three pressures when IFT is reduced by about 50%.

4. Conclusion and Future Perspective

In order to quantitatively investigate the mechanisms and contributing factors of the contact angle alteration of the CO_2/brine/muscovite system caused by the change in pressure, the disjoining pressure curves and the contact angle were calculated both at three pressure cases, i.e., 0.1 MPa, 3.0 MPa, and 10.0 MPa.

The results obtained were consistent with the trends of the data of the contact angle reported in previous studies. From 0.1 MPa to 3.0 MPa, about 80% to 90% of the decrease of the potential energy was caused by the change in Π_{hyd}, which was due to the decrease in pH. From 3.0 MPa to 10.0 MPa, the pH does not change much, and the decrease in the potential energy was mostly caused by the change in Π_{vdW}, which is related to an increase in CO_2 density. The IFT decreased by 26.4% from 0.1 MPa to 3.0 MPa, and it decreased by 36.0% from 3.0 MPa to 10.0 MPa. Therefore, it can be said that pH decrease is the key contributing factor in the lower pressure region, while an increase in CO_2 density and IFT decrease are the ones in the higher pressure region. Sensitivity analysis also shows that the contact angle is sensitive to the interfacial

Table 2: The number of references in the legend of Figure 6.

Number	Reference	Temperature	Salinity	Type of measurement**
1	Chiquet et al. (2007) [3]	308 K	0.01 M	R
2			0.1 M	
3			0.2 M	
4			0.5 M	
5			1 M	
6	Broseta et al. (2012) [4]	308 K	0.01 M	A
7				R∗
8				A
9			0.08 M	R
10		282 K		A
11				R
12	Mills et al. (2011) [43]	313 K	35000 ppm	S
13				A
14				R
15	Farokhpoor et al. (2013) [5]	309 K	0.8 M	A

** indicates the following: S = static angle; R = receding angle; R∗ = nonequilibrated receding angle; A = advancing angle.

tension of CO_2/brine and the physical properties of hydration forces.

Further measurements of physical properties related to CO_2, brine, and other minerals are expected in the study of wettability in a broader range of conditions. Moreover, further investigation into interactions from an atomic viewpoint will help us to have a better understanding of sensitive parameters such as the coefficient of hydration forces..

Data Availability

Data for all the calculations are available through previously reported articles. These prior studies are cited at relevant places within the text as references.

Additional Points

Key Points. (i) Contact angle of the CO_2/brine/muscovite system was calculated with increasing pressure, by the Frumkin-Derjaguin equation. (ii) The decrease in pH, the increase in CO_2 density, and the decrease in the interfacial tension of CO_2/brine were the crucial factors. (ii) Results were sensitive to the interfacial tension of CO_2/brine and the coefficient of the model for the hydration forces.

Conflicts of Interest

The authors declare that they have no conflicts of interest.

Acknowledgments

The authors are grateful for Professor George Hirasaki for giving us important comments and suggestions so that the article improved very much. The authors are also thankful for Dr. S.V. Lin and Professor F. Mugele for answering our questions about their article, which has a key role in this work.

Supplementary Materials

Figures S1 and S2: detailed explanation of the method. Figure S3: details of the calculation results related to $\Pi_{vdW}(h)$. Figures S4 and S5 and Text S1: details of the calculation results related to $\Pi_{ele}(h)$. Figure S6: details of the calculation results related to $\Pi_{hyd}(h)$. Figures S7–S10 and Tables S1–S7: detailed figures related to $W(h)$. Figures S11 and S12: contact angles with changes in the surface electrical potentials at 0.1 MPa and 3.0 MPa. *(Supplementary Materials)*

References

[1] P. H. Nelson, "Pore-throat sizes in sandstones, tight sandstones, and shales," *AAPG Bulletin*, vol. 93, no. 3, pp. 329–340, 2009.

[2] S. Iglauer, C. H. Pentland, and A. Busch, "CO_2 wettability of seal and reservoir rocks and the implications for carbon geo-sequestration," *Water Resources Research*, vol. 51, no. 1, pp. 729–774, 2015.

[3] P. Chiquet, J. L. Daridon, D. Broseta, and S. Thibeau, "CO_2/water interfacial tensions under pressure and temperature conditions of CO_2 geological storage," *Energy Conversion and Management*, vol. 48, no. 3, pp. 736–744, 2007.

[4] D. Broseta, N. Tonnet, and V. Shah, "Are rocks still water-wet in the presence of dense CO_2 or H_2S?," *Geofluids*, vol. 12, no. 4, pp. 280–294, 2012.

[5] R. Farokhpoor, B. J. Bjørkvik, E. Lindeberg, and O. Torsæter, "Wettability behaviour of CO_2 at storage conditions," *International Journal of Greenhouse Gas Control*, vol. 12, pp. 18–25, 2013.

[6] M. Arif, A. Z. Al-Yaseri, A. Barifcani, M. Lebedev, and S. Iglauer, "Impact of pressure and temperature on CO_2-brine-mica contact angles and CO_2-brine interfacial tension: implications for carbon geo-sequestration," *Journal of Colloid and Interface Science*, vol. 462, pp. 208–215, 2016.

[7] G. J. Hirasaki, "Thermodynamics of thin films and three-phase contact regions," in *Interfacial Phenomena in Oil Recovery*, N. R. Morrow, Ed., pp. 23–76, Marcel Dekker, Inc,, 1991.

[8] M. J. Alshakhs and A. R. Kovscek, "Understanding the role of brine ionic composition on oil recovery by assessment of wettability from colloidal forces," *Advances in Colloid and Interface Science*, vol. 233, pp. 126–138, 2016.

[9] A. Sanaei and K. Sepehrnoori, "Implication of oil/brine/rock surface interactions in modeling modified salinity waterflooding in carbonate and sandstone reservoirs," in *SPE Annual Technical Conference and Exhibition*, Texas, USA, September 2018Society of Petroleum Engineers.

[10] A. Frumkin, "Phenomena of wetting and adhesion of bubbles," *I. Zhurnal Fizicheskoi Khimii*, vol. 12, no. 337, pp. 337–345, 1938.

[11] B. V. Derjaguin, "Theory of the capillary condensation and other capillary phenomena taking into account the disjoining effect of long-chain molecular liquid films," *Zhurnal Fizicheskoi Khimii*, vol. 14, p. 137, 1940.

[12] J. N. Israelachvili and R. M. Pashley, "Molecular layering of water at surfaces and origin of repulsive hydration forces," *Nature*, vol. 306, no. 5940, pp. 249-250, 1983.

[13] V. Médout-Marère, "A simple experimental way of measuring the Hamaker constant A_{11} of divided solids by immersion calorimetry in apolar liquids," *Journal of Colloid and Interface Science*, vol. 228, no. 2, pp. 434–437, 2000.

[14] J. N. Israelachvili and D. Tabor, "The measurement of van der Waals dispersion forces in the range 1.5 to 130 nm," *Proceedings of the Royal Society of London. A. Mathematical and Physical Sciences*, vol. 331, no. 1584, pp. 19–38, 1972.

[15] D. B. Hough and L. R. White, "The calculation of Hamaker constants from Liftshitz theory with applications to wetting phenomena," *Advances in Colloid and Interface Science*, vol. 14, no. 1, pp. 3–41, 1980.

[16] J. Gregory, "The calculation of Hamaker constants," *Advances in Colloid and Interface Science*, vol. 2, no. 4, pp. 396–417, 1970.

[17] J. Visser, "On Hamaker constants: a comparison between Hamaker constants and Lifshitz-van der Waals constants," *Advances in Colloid and Interface Science*, vol. 3, no. 4, pp. 331–363, 1972.

[18] L. Bergström, "Hamaker constants of inorganic materials," *Advances in Colloid and Interface Science*, vol. 70, pp. 125–169, 1997.

[19] Y. Sun, B. Y. Shekunov, and P. York, "Refractive index of supercritical CO_2-ethanol solvents," *Chemical Engineering Communications*, vol. 190, no. 1, pp. 1–14, 2003.

[20] T. Moriyoshi, T. Kita, and Y. Uosaki, "Static relative permittivity of carbon dioxide and nitrous oxide up to 30 MPa," *Berichte der Bunsengesellschaft für Physikalische Chemie*, vol. 97, no. 4, pp. 589–596, 1993.

[21] D. J. Bradley and K. S. Pitzer, "Thermodynamics of electrolytes. 12. Dielectric properties of water and Debye-Huckel parameters to 350°C and 1 kbar," *Journal of Physical Chemistry*, vol. 83, no. 12, pp. 1599–1603, 1979.

[22] A. H. Harvey, J. S. Gallagher, and J. L. Sengers, "Revised formulation for the refractive index of water and steam as a function of wavelength, temperature and density," *Journal of Physical and Chemical Reference Data*, vol. 27, no. 4, pp. 761–774, 1998.

[23] L. Weiss, A. Tazibt, A. Tidu, and M. Aillerie, "Water density and polarizability deduced from the refractive index determined by interferometric measurements up to 250 MPa," *The Journal of Chemical Physics*, vol. 136, no. 12, p. 124201, 2012.

[24] N. M. Balzaretti, J. P. Denis, and J. A. H. Da Jornada, "Variation of the refractive index and polarizability of sapphire under high pressures," *Journal of Applied Physics*, vol. 73, no. 3, pp. 1426–1429, 1993.

[25] R. T. W. D. W. Hogg, T. W. Healy, and D. W. Fuerstenau, "Mutual coagulation of colloidal dispersions," *Transactions of the Faraday Society*, vol. 62, pp. 1638–1651, 1966.

[26] S. Usui, "Interaction of electrical double layers at constant surface charge," *Journal of Colloid and Interface Science*, vol. 44, no. 1, pp. 107–113, 1973.

[27] G. J. Hirasaki, "Wettability: fundamentals and surface forces," *SPE Formation Evaluation*, vol. 6, no. 2, pp. 217–226, 2013.

[28] U. Alonso, T. Missana, H. Geckeis et al., "Role of inorganic colloids generated in a high-level deep geological repository in the migration of radionuclides: open questions," *Journal of Iberian Geology*, vol. 32, no. 1, pp. 79–94, 2006.

[29] P. I. Au, S. Y. Siow, L. Avadiar, E. M. Lee, and Y. K. Leong, "Muscovite mica and koalin slurries: yield stress-volume fraction and deflocculation point zeta potential comparison," *Powder Technology*, vol. 262, pp. 124–130, 2014.

[30] W. Zhou, J. Niu, W. Xiao, and L. Ou, "Adsorption of bulk nanobubbles on the chemically surface-modified muscovite minerals," *Ultrasonics Sonochemistry*, vol. 51, pp. 31–39, 2019.

[31] M. S. Kim and D. H. Kwak, "Effect of zeta potential on collision-attachment coefficient and removal efficiency for dissolved carbon dioxide flotation," *Environmental Engineering Science*, vol. 34, no. 4, pp. 272–280, 2017.

[32] S. R. Van Lin, K. K. Grotz, I. Siretanu, N. Schwierz, and F. Mugele, "Ion-specific and pH-dependent hydration of mica-electrolyte interfaces," *Langmuir*, vol. 35, no. 17, pp. 5737–5745, 2019.

[33] A. V. Nguyen, J. Drelich, M. Colic, J. Nalaskowski, and D. Miller Jan, *Bubbles: interaction with solid surfaces*, P. Somasundaran, Ed., Encyclopedia of Surface and Colloid Science, Taylor and Francis, London, 2007.

[34] E. W. Lemmon, M. O. McLinden, and D. G. Friend, "Thermophysical properties of fluid systems," in *NIST Chemistry WebBook, NIST standard reference database number 69*, P. J. Linstrom and W. G. Mallard, Eds., National Institute of Standards and Technology, Gaithersburg MD, USA, 2017.

[35] W. B. Floriano and M. A. C. Nascimento, "Dielectric constant and density of water as a function of pressure at constant temperature," *Brazilian Journal of Physics*, vol. 34, no. 1, pp. 38–41, 2004.

[36] H. T. Schaeff and B. P. McGrail, "Direct measurements of pH in H_2O-CO_2 brine mixtures to supercritical conditions," in *Proceedings of the 7th International Conference on Greenhouse Gas Control Technologies (GHGT-7)*, pp. 2169–2173, Vancouver, Canada, 2004.

[37] L. Cheng, P. Fenter, K. L. Nagy, M. L. Schlegel, and N. C. Sturchio, "Molecular-scale density oscillations in water adjacent to a mica surface," *Physical Review Letters*, vol. 87, no. 15, p. 156103, 2001.

[38] H. Sakuma, T. Kondo, H. Nakao, K. Shiraki, and K. Kawamura, "Structure of hydrated sodium ions and water molecules adsorbed on the mica/water interface," *The Journal of Physical Chemistry C*, vol. 115, no. 32, pp. 15959–15964, 2011.

[39] S. S. Lee, P. Fenter, K. L. Nagy, and N. C. Sturchio, "Monovalent ion adsorption at the muscovite (001)-solution interface: relationships among ion coverage and speciation, interfacial

water structure, and substrate relaxation," *Langmuir*, vol. 28, no. 23, pp. 8637–8650, 2012.

[40] H. Sakuma and K. Kawamura, "Structure and dynamics of water on Li+-, Na+-, K+-, Cs+-, H_3O+-exchanged muscovite surfaces: a molecular dynamics study," *Geochimica et Cosmochimica Acta*, vol. 75, no. 1, pp. 63–81, 2011.

[41] K. Kobayashi, Y. Liang, K. I. Amano et al., "Molecular dynamics simulation of atomic force microscopy at the water-muscovite interface: hydration layer structure and force analysis," *Langmuir*, vol. 32, no. 15, pp. 3608–3616, 2016.

[42] A. Georgiadis, G. Maitland, J. M. Trusler, and A. Bismarck, "Interfacial tension measurements of the (H_2O+CO_2) system at elevated pressures and temperatures," *Journal of Chemical & Engineering Data*, vol. 55, no. 10, pp. 4168–4175, 2010.

[43] J. Mills, M. Riazi, and M. Sohrabi, "Wettability of common rock-forming minerals in a CO_2-brine system at reservoir conditions," in *International Symposium of the Society of Core Analysts*, pp. 19–21, Society of Core Analysts Fredericton, Canada, 2011.

[44] H. D. Ackler, R. H. French, and Y. M. Chiang, "Comparisons of Hamaker constants for ceramic systems with intervening vacuum or water: from force laws and physical properties," *Journal of Colloid and Interface Science*, vol. 179, no. 2, pp. 460–469, 1996.

[45] F. Mugele, B. Bera, A. Cavalli et al., "Ion adsorption-induced wetting transition in oil-water-mineral systems," *Scientific Reports*, vol. 5, no. 1, p. 10519, 2015.